Interaction of carbon nanotubes with microbial enzymes: conformational transitions and potential toxicity

Ming Chen, [a,b,*] Guangming Zeng, [a,b,*] Piao Xu, [a,b] Min Yan, [a,b] Weiping Xiong [a,b] and Shuang Zhou [a,b]

[a]*College of Environmental Science and Engineering, Hunan University, Changsha 410082, China*

[b]*Key Laboratory of Environmental Biology and Pollution Control (Hunan University), Ministry of Education, Changsha 410082, China*

Keywords: carbon nanotube; nanotoxicity; protein-protein interaction; microbe.

[*]Corresponding author. E-mail: mchensn@hnu.edu.cn (M. Chen) and zgming@hnu.edu.cn (G. Zeng)

Abstract

Wide industrial, environmental and biomedical applications of carbon nanotubes (CNTs) are bringing them to enter the environment. Their toxicity to microorganisms has been experimentally reported, but underlying molecular mechanism is still unclear. Here, we investigated conformational transitions in widely distributed microbial enzymes in the presence and absence of single-walled carbon nanotubes (SWCNTs) by molecular dynamics (MD) simulations. Our study identifies a new mechanism that SWCNTs produce possible toxicity to microbes by inducing significant changes in enzymatic conformations. The protein-protein interactions undergo significant transitions with two monomers either towards or away from each other upon the appearance of SWCNTs. The significant conformational changes in microbial enzymes may inactivate the microbial enzymes and disturb the microbial metabolism.

Introduction

Carbon nanotubes (CNTs), as promising materials with unique mechanical, optical, chemical properties, have been added into various products [1-3]. The toxicity assessment of carbon-based nanomaterials to living organisms is becoming important before they can be produced for applications [4-7], which requires a more thorough understanding of mechanisms causing the toxicity at the molecular level. Currently, the ecological safety and environmental concerns over the carbon-based nanomaterials have become a hot research subject. Environmental release of CNTs can be unintentional but sometimes may be purposeful during their production and use. Their behaviour in the environment is still largely unclear.

Carbon-based nanomaterials are toxic to some microbes [8, 9]. For example, low concentration of graphene oxide is helpful in the growth of *Phanerochaete chrysosporium*, but the high one will break its fiber structure and make it inactive [10]. In addition to toxicity to microbes, carbon-based nanomaterials also exhibited toxicity to other organisms, such as animals. Using genome-wide gene expression analysis, SWCNT's toxic molecular mechanism to *Caenorhabditis elegans* was evaluated by Chen et al. [11], which showed that amide-modified SWCNTs induce toxicity to the worms by several pathways, e.g., reduction of citrate cycle activity and defective endocytosis. It seems that there are no 100% safe carbon nanomaterials [12]. While several studies have investigated the cytotoxicity and organ toxicity of nanomaterials [13-15], where the interactions of nanomaterials with proteins were believed to be

precondition for the toxicity, the molecular-level interaction mechanism between nanomaterials and proteins remain unclear especially in microbes, and must be further explored. In addition, protein-protein interactions need to be concerned, because proteins often work together to perform their functions by interacting with each other [16].

Microbial functions depend strongly on their enzymes. For instance, lignin degradation by *P. chrysosporium* is achieved relying on its secreted manganese peroxidase (MnP) and lignin peroxidase (LiP) [17, 18]. Other important microbial functions such as reproduction, development, nutrient uptake and growth need the participation of enzymes.

Recently, we observed conformational changes in LiP and MnP of *P. chrysosporium*, laccases of *Trametes versicolor* and *Melanocarpus albomyces*, naphthalene 1,2-dioxygenase of *Pseudomonas* sp. C18, and haloalkane dehalogenase of *Sphingobium* sp. MI1205 upon exposure to SWCNTs [19, 20]. Moreover, graphene [16] and graphene oxide [21] present potential toxicity to biological cells by disrupting the interaction between protein and protein. These previous findings suggest that CNTs may produce potential toxicity to microbes by inducing conformational changes in proteins or enzymes. Our goal in the present study is to determine whether enzymatic conformations will be strongly affected by SWCNTs, simultaneously focusing on the protein-protein interactions. To achieve this purpose, we chose two microbial

enzymes with each containing two chains. A (6,5)-SWCNT was put at the position near the middle part of two chains for each enzyme.

Materials and methods

Crystal structures of maleylpyruvate isomerase (MPI) from bacteria *Ralstonia* sp. u2 (2V6K [22]) and lignin peroxidase (LiP) from fungus *Phanerochaete chrysosporium* (1QPA [23]) were downloaded from RCSB PDB [24] (http://www.rcsb.org/pdb/home/home.do). These two structures are homo-dimer with total structure weights of 48475.36 and 76851.09, respectively. Each of them is composed of two chains: 214 amino acids and 345 amino acids for each chain of MPI and LiP, respectively. Non-protein parts of these two structures were removed. Structure model of (6,5)-SWCNT was produced using VMD [25].

The initial conformations of the SWCNT complexed with MPI and LiP were produced by positioning the SWCNT near the binding region of two chains, respectively. The reason that we put the SWCNT at this position is because this binding region may be relatively easily affected by the SWCNTs compared with other regions inside the proteins. The MPI and LiP without the SWCNT were used as the control groups. For simplicity, the system containing the SWCNT and LiP is called LiP+SWCNT, while that containing only LiP is called LiP-no-SWCNT. Similarly, MPI+SWCNT and MPI-no-SWCNT correspond to the systems with and without the SWCNT, respectively. These four systems were neutralized by genion software which

is a part of GROMACS [26] and energy-minimized using steepest descent method after they were solvated with SPC water model [27]. The total atom number is 140011 for MPI+SWCNT, 162237 for LiP+SWCNT, 140187 for MPI-no-SWCNT, and 162446 for LiP-no-SWCNT. Sixty nanosecond (ns) MD simulation was carried out for each system by the software package GROMACS V-4.60 [26] with OPLS-AA force field [28]. Three-dimension periodic boundary conditions were used. In the present study, 60 ns was found enough for observing the dynamic interactions between the SWCNT and microbial enzymes. Indeed, several previous studies preferred 30-60 ns to investigate the interactions between carbon nanomaterials and proteins [16, 19, 29]. The MD trajectories were explored using VMD [25] and GROMACS [26]. Cavity volume of protein cavities and the solvent molecule number overlapping the cavities were calculated by trj_cavity [30]. Two-tailed paired *t* tests were carried out based on all data over the entire time-sequence to determine if the SWCNT affected the distance between the center of mass of two chains (D), radius of gyration (Rg), cavity volume and the solvent molecule number overlapping the cavities, respectively. Microsoft Excel was used for these analyses.

Results and discussion

The real exposing scenarios for CNTs to living organisms have been investigated in several previous studies, which focused on their response to CNTs [31], variations in stability or activity of enzymes [32], and change in microbial community composition in soil [33], activated sludge [34], and other sites. However, there are few studies on the

molecular mechanism that CNTs cause this toxicity from the view point of enzymes. Protein-nanomaterial interactions have been considered as a precondition for the cytotoxicity of nanomaterials [13]. Thus, we hypothesized that potential toxicity of SWCNTs to microbes may be linked to structural change in microbial proteins or enzymes. To answer the question whether our hypothesis is correct, we compared the conformational differences between the same enzyme with and without the SWCNT by two-tailed paired *t* test. The real exposing scenarios for CNTs to enzymes are more complex than the present scenario that consider the interaction of single SWCNT with enzymes. For example, CNTs are likely to be highly aggregated and coated by other biofilms in practical situations. However, at the molecular level, enzymes may only touch one molecule of CNT aggregates. Thus, our present results can be used to explain the molecular-level interactions between CNTs and enzymes in the real scenarios.

The data on conformational change in enzyme with time was obtained by MD simulations which have been confirmed to be a useful tool in determining the impacts of nanomaterials on protein structures [16, 19, 20, 35, 36]. The types of microbial enzymes are very diverse. It is impossible to include all microbial enzymes in the present study. Thus, we selected two enzymes (LiP from *P. chrysosporium* and MPI from *Ralstonia* sp. u2), whose 3D structures have been determined experimentally. These two enzymes exist in a wide range of microbes in addition to the above two microorganisms, e.g., LiP is also detected in *Acinetobacter calcoaceticus* NCIM 2890

[37], *Brevibacillus laterosporus* MTCC 2298 [38], *Gloeophyllum sepiarium* MTCC-1170 [39], *Trametes versicolor* IBL-04 [40], *etc*. In addition, MPI is also found in diverse microbes, e.g., *Arthrobacter* sp. scl-2 [41] and *Klebsiella pneumoniae* M5a1 [42]. Another very important reason that we selected these two enzymes is due to their 3D structures composed of two chains, which allows us to observe protein-protein interaction [16]. In the case without SWCNTs, the whole LiP or MPI exhibited stable behaviour as shown by the backbone root-mean-square deviation (RMSD) (Figure 1a) with an average RMSD of 0.23 nm for LiP and of 0.17 nm for MPI; in addition, each chain of LiP or MPI rapidly reached equilibrium over 60-ns simulations (Figure 1b and c). The behaviour of LiP and MPI may be changed by SWCNTs, and is demonstrated below.

LiP

LiP is one of ligninolytic enzymes [18]. LiP from *P. chrysosporium* can metabolism several types of pollutants [43]. In particular, carboxylated SWCNTs is able to be degraded by LiP from *Sparassis latifolia* [44], but pristine SWCNTs cannot be degraded by LiP from *P. chrysosporium* [45]. Thus, in this study, we selected LiP from *P. chrysosporium* and pristine SWCNT to avoid this interference factor because our purpose is not related to biodegradation of CNTs in this study. As to SWCNTs, in this study, we have used (6,5)-SWCNT that was previously adopted in studies related to tumor imaging and photothermal therapy [46] and the enrichment of SWCNTs by surfactants [47] and genomic DNA [48].

The simulated systems at 0 ns containing only LiP (LiP-no-SWCNT) and LiP+SWCNT are shown in Figure 2A and B, respectively. The systems without the SWCNT were used as the control groups. At the begin of the simulation, the SWCNT is at the position near the binding part between chains A and B of LiP and in a direction substantially parallel with the axis of this binding part. The whole LiP in the presence of SWCNT showed stable behaviour, as revealed by the backbone RMSDs (Figure 1d); moreover, each chain of LiP also reached equilibrium during the simulations (Figure 1e). D was calculated with and without the SWCNT, which is significantly different under these two conditions ($P < 0.01$) based on two-tailed paired *t* test. Figure 2C shows that D is bigger in LiP-no-CNT than in LiP+SWCNT during most of the simulation time. The appearance of SWCNT leads to about an average decrease of 0.07 nm in D. However, the decrease does not mean that LiP becomes more stable. By contrast, LiP becomes more unstable in the present of SWCNT, as reflected by Figure 2C, where the curve for LiP+SWCNT fluctuates more dramatically as compared to that for LiP-no-CNT. Thus, the significant conformational changes in LiP has happened after the incorporation of SWCNT. This is also confirmed by the result about radius of gyration (Rg) which is significantly different between LiP-no-SWCNT and LiP+SWCNT (two-tailed *t* test: $P < 0.01$) (Figure 2D). The significant difference in Rg between these two systems indicated that the structural compactness in the LiP has been changed by the SWCNT, because Rg determines the structural compactness of proteins [49]. In particular, the structural

compactness of LiP showed a maximum difference at about 35 ns between LiP-no-SWCNT and LiP+SWCNT. In addition, significant conformational changes were also observed in local regions of LiP, as shown by the cavity volume (two-tailed *t* test: $P < 0.01$), where the SWCNT caused the expansion of LiP cavities, especially after 20 ns (Figure 2E). Correspondingly, the solvent molecule number overlapping the cavities in LiP+SWCNT was generally more than in LiP-no-SWCNT (Figure 2F).

It is possible that the binding part of chains A and B in LiP has a more obvious conformational transformation because the SWCNT was positioned near it and the connection between two chains is relatively weak as compared to that between any parts from the same chain. Thus, we have a careful look at this binding part by extracting the 5 Å region within both chains A and B at 3, 20 40 and 60 ns (Figure 3). Figure 3a, e and i show that the SWCNT induces an obvious structural changes in the binding part of chains A and B, attracting 136 more atoms to this 5 Å binding regions at 3 ns. In addition, some helix structures start to appear in chain A due to the presence of SWCNT. It must be noted that one end of the SWCNT is still very close to chain A at 3 ns. At 20 ns, the atom number and residue number are very similar under two conditions with and without the SWCNT, respectively; the orientation of the SWCNT has been completely changed and one end of the SWCNT is near the chain B (Figure 3b and f). The SWCNT moved away from both chains A and B at 40 ns. The atom number in the binding region becomes comparable (1042 for LiP-no-SWCNT and 1030 for LiP+SWCNT) with the same residue number (80 for

each of them) at 40 ns (Figure 3c, g and i). At the end of 60-ns simulations, more atoms moved to the binding region in LiP-no-SWCNT and LiP+SWCNT (Figure 3d, h and i). The SWCNT brought more atoms and residues into the 5 Å region around both chains A and B.

MPI

Following the study of LiP, another enzyme MPI is selected to confirm the above finding that the presence of SWCNTs would significantly transform the microbial enzymes' conformations. The structure of MPI is totally different from that of LiP, because the gap in the binding part of chains A and B for MPI is obviously smaller than that for LiP, as reflected by the smaller mean D in MPI than in LiP (2.3 nm vs. 3.6 nm). Clearly, there is almost no gap in the binding part of chains A and B for MPI (Figure 4A). Can this very close binding protect the enzyme from external interference of the SWCNT? To answer this question, two systems were developed: MPI-no-SWCNT and MPI+SWCNT. The MPI-no-SWCNT was used for comparative purpose. The whole MPI or each chain of MPI with the SWCNT was well-equilibrated during the whole simulations (Figure 1d and f). The SWCNT was initially positioned near the binding part of chains A and B of MPI (Figure 4B). The almost seamless connection between chains A and B failed to protect the MPI from the interference of the SWCNT, as shown by that the D for MPI has been significantly changed by the SWCNT (two-tailed *t* test: $P < 0.01$) (Figure 4C). This failure is also supported by the significant transformation in Rg between MPI-no-SWCNT and

MPI+SWCNT (two-tailed *t* test: $P < 0.01$) (Figure 4D). The SWCNT led to a less tight packing in MPI with an average increase of about 0.01 nm in Rg. The cavity volume of MPI is, however, not significantly affected by the SWCNT (two-tailed *t* test: $P = 0.059$) (Figure 4E). Despite insignificance, it must be noted that the curve for cavity volume of MPI-no-SWCNT and the curve for that of MPI+SWCNT is inconsistent and that the *P* value is very close to the significant level 0.05. Moreover, the solvent occupancy of the cavities is observed to be significantly different (two-tailed *t* test: $P < 0.01$) between MPI-no-SWCNT and MPI+SWCNT, where the solvent molecule number overlapping the cavities decreases about 285 after the appearance of the SWCNT (Figure 4F). At the end of 60-ns simulation, the initial orientation of the SWCNT has been completely altered, the enzyme structure in MPI+SWCNT becomes more loose with a larger D and Rg compared with that in MPI-no-SWCNT.

To observe conformational change more clearly, we focused on the 5 Å region within both chains A and B which is their binding part (Figure 5). The presence of the SWCNT has changed the shape of this part, as reflected by the increase or decrease in atom and residue number of this region. Similar to LiP, the SWCNT forced 122 more atoms and 5 more residues into this region at 3 ns (Figure 5a, e and i). The trend at 20 ns is opposite to that at 3 ns, where the atom and residue number in this 5 Å region is more in MPI-no-SWCNT than in MPI+SWCNT (Figure 5b, f and i). The different variation patterns in atom and residue number continued with time, e.g., at 40 ns

(Figure 5c and g) and 60 ns (Figure 5d and h). Interestingly, a β-sheet (shown by solid arrow) always existed in chain B of MPI-no-SWCNT during the whole simulation. A β-sheet also appeared in chain B of MPI+SWCNT in most of time, but finally disappeared. In particular, the β-sheet in chain B of MPI+SWCNT looks smaller and thinner than that of MPI-no-SWCNT. Xu et al. also observed the structural conversion in the lysozyme protein by nanomaterials but from an α-helix into a β-sheet [13]

Potential molecular basis for the toxicity of CNTs to microbes

Based on the above findings, herein, we identified a potential molecular basis for the toxicity of CNTs to microbes, which was not reported previously, although a lot of studies have found that CNTs are toxic to microbes [31, 33, 34]. That is, CNTs bind to microbial enzymes, and produce toxicity to the microbes by inducing significant conformational changes in enzymes based on the following facts:

1. The SWCNTs caused significant conformational changes in widely distributed microbial enzymes, as shown by the current study. It was reported that functionalized CNTs could interacted with α-chymotrypsin and further inhibited the protein's enzymatic activity [50]. Conformational changes in proteins after the incorporation of nanomaterials were also reported in several other studies [13, 51, 52]. Given that microbial metabolism relies on their secreted enzymes, conformational change in proteins will affect the metabolic processes, such as cellular uptake, decomposition and clearance of the nanomaterials [53]. The conformational change in enzymes can be global, as

reflected by the packing of the enzymes becomes more or less tight (Figures 2D and 4D). Moreover, this change also can be local. For example, the SWCNT can adjust the cavity volume of the enzymes and further affect the solvent molecule number that overlapping the cavities. The enzymatic cavities are often active sites or pockets bound to the substrate molecules [30]. Cavity variations in the enzymes thus will interfere with the enzymatic reactions.

2. Microbial protein-protein interaction patterns are significantly changed by the SWCNT, as shown by the D for LiP and MPI (Figures 2C and 4C). Our results based on the SWCNT are different from those based on graphene [16] or graphene oxide [21] where they can insert into the dimer. This can be expected, since the cylindric SWCNT is very hard to cross the narrow binding part between two proteins, while graphene or graphene oxide is planar and thus easy to enter this binding part. Indeed, a previous study from the same group also found that CNT and graphene exhibited different interactional behaviour with protein villin headpiece (HP35), and the nanomaterial shapes are important to the interact between nanomaterials and protein [54].

Conclusions

Our results demonstrate that significant conformational transformations in two widely distributed microbial enzymes (LiP and MPI) are induced by the SWCNTs. These transformations include backbone fluctuations, protein compactness changes and the

adjustment of protein cavities. In particular, the presence of SWCNTs can interfere the microbial protein-protein interactions. Significant changes in enzyme conformations may inhibit enzymatic functions and break microbial metabolism, which can be a potential mechanism for explaining the experimentally observed toxicity of CNTs to microbes at the molecular level.

Acknowledgments

The study was financially supported by the National Natural Science Foundation of China (51508177, 51521006, 51378190), and the Program for Changjiang Scholars and Innovative Research Team in University (IRT-13R17).

References

1. M. Chen, X. Qin and G. Zeng, *Trends Biotechnol*, 2017, DOI: 10.1016/j.tibtech.2016.1012.1001.
2. M. F. De Volder, S. H. Tawfick, R. H. Baughman and A. J. Hart, *Science*, 2013, **339**, 535-539.
3. X. Fan, C. Yu, Z. Ling, J. Yang and J. Qiu, *Acs Appl Mater Inter*, 2013, **5**, 2104-2110.
4. R. S. Chouhan, A. Qureshi, B. Yagci, M. A. Gülgün, V. Ozguz and J. H. Niazi, *Chem Eng J*, 2016, **298**, 1-9.
5. S. Lanone, P. Andujar, A. Kermanizadeh and J. Boczkowski, *Adv Drug Delivery Rev*, 2013, **65**, 2063-2069.

6. M. Ema, K. S. Hougaard, A. Kishimoto and K. Honda, *Nanotoxicology*, 2016, **10**, 391-412.

7. J. Zhao, Z. Wang, J. C. White and B. Xing, *Environ Sci Technol*, 2014, **48**, 9995-10009.

8. C. D. Vecitis, K. R. Zodrow, S. Kang and M. Elimelech, *ACS Nano*, 2010, **4**, 5471-5479.

9. S. Kang, M. S. Mauter and M. Elimelech, *Environ Sci Technol*, 2009, **43**, 2648-2653.

10. J. Xie, Z. Ming, H. Li, H. Yang, B. Yu, R. Wu, X. Liu, Y. Bai and S.-T. Yang, *Chemosphere*, 2016, **151**, 324-331.

11. P.-H. Chen, K.-M. Hsiao and C.-C. Chou, *Biomaterials*, 2013, **34**, 5661-5669.

12. P. Begum, R. Ikhtiari and B. Fugetsu, *Carbon*, 2011, **49**, 3907-3919.

13. Z. Xu, X.-W. Liu, Y.-S. Ma and H.-W. Gao, *Environ Sci Pollut R*, 2010, **17**, 798-806.

14. L.-C. Cheng, X. Jiang, J. Wang, C. Chen and R.-S. Liu, *Nanoscale*, 2013, **5**, 3547-3569.

15. G. Maiorano, S. Sabella, B. Sorce, V. Brunetti, M. A. Malvindi, R. Cingolani and P. P. Pompa, *Acs Nano*, 2010, **4**, 7481-7491.

16. B. Luan, T. Huynh, L. Zhao and R. Zhou, *Acs Nano*, 2015, **9**, 663-669.

17. D. L. Huang, G. Zeng, C. L. Feng, S. Hu, X. Y. Jiang, L. Tang, F. F. Su, Y. Zhang, W. Zeng and H. L. Liu, *Environ Sci Technol*, 2008, **42**, 4946-4951.

18. M. Chen, G. Zeng, Z. Tan, M. Jiang, H. Li, L. Liu, Y. Zhu, Z. Yu, Z. Wei, Y. Liu and G. Xie, *PLoS ONE*, 2011, **6**, e25647.

19. M. Chen, X. Qin, J. Li and G. Zeng, *RSC Adv.*, 2016, **6**, 3592 - 3599.

20. M. Chen, X. Qin and G. Zeng, *Chemosphere*, 2016, **163**, 217-226.

21. M. Feng, H. Kang, Z. Yang, B. Luan and R. Zhou, *J Chem Phys*, 2016, **144**, 225102.

22. M. Marsh, D. K. Shoemark, A. Jacob, C. Robinson, B. Cahill, N. Y. Zhou, P. A. Williams and A. T. Hadfield, *J Mol Biol*, 2008, **384**, 165-177.

23. T. Choinowski, W. Blodig, K. H. Winterhalter and K. Piontek, *J Mol Biol*, 1999, **286**, 809-827.

24. P. W. Rose, A. Prlić, C. Bi, W. F. Bluhm, C. H. Christie, S. Dutta, R. K. Green, D. S. Goodsell, J. D. Westbrook and J. Woo, *Nucleic Acids Res*, 2015, **43**, D345-D356.

25. W. Humphrey, A. Dalke and K. Schulten, *J Mol Graph*, 1996, **14**, 33-38.

26. B. Hess, C. Kutzner, D. van der Spoel and E. Lindahl, *J Chem Theory Comput*, 2008, **4**, 435-447.

27. H. Berendsen, J. Postma, W. Van Gunsteren and J. Hermans, Intermolecular Forces, *Reidel, Dordrecht*, 1981, pp: 331-342.

28. G. A. Kaminski, R. A. Friesner, J. Tirado-Rives and W. L. Jorgensen, *The Journal of Physical Chemistry B*, 2001, **105**, 6474-6487.

29. M. Calvaresi, S. Hoefinger and F. Zerbetto, *Chem-Eur J*, 2012, **18**, 4308-4313.

30. T. Paramo, A. East, D. Garzón, M. B. Ulmschneider and P. J. Bond, *J Chem Theory Comput*, 2014, **10**, 2151-2164.

31. A. Simon-Deckers, S. Loo, M. Mayne-L'hermite, N. Herlin-Boime, N. Menguy, C. Reynaud, B. Gouget and M. Carrière, *Environ Sci Technol*, 2009, **43**, 8423-8429.

32. P. Du, J. Zhao, H. Mashayekhi and B. Xing, *J. Phys. Chem. C*, 2014, **118**, 22249-22257.

33. L. Jin, Y. Son, J. L. DeForest, Y. J. Kang, W. Kim and H. Chung, *Sci Total Environ*, 2014, **466**, 533-538.

34. D. Goyal, X. Zhang and J. Rooney‐Varga, *Lett Appl Microbiol*, 2010, **51**, 428-435.

35. M. Chen, G. Zeng, P. Xu, Y. Zhang, D. Jiang and S. Zhou, *Environmental Science: Nano*, 2017.

36. M. Chen, G. Zeng, C. Lai, C. Zhang, P. Xu, M. Yan and W. Xiong, *Chemosphere*, 2017, https://doi.org/10.1016/j.chemosphere.2017.1005.1162.

37. G. S. Ghodake, S. D. Kalme, J. P. Jadhav and S. P. Govindwar, *Appl Biochem Biotech*, 2009, **152**, 6-14.

38. S. S. Gomare, J. P. Jadhav and S. P. Govindwar, *Biotechnol Bioproc E*, 2008, **13**, 136-143.

39. M. Yadav, P. Yadav and K. Yadav, *Biochemistry (Moscow)*, 2009, **74**, 1125-1131.

40. M. Asgher, H. M. N. Iqbal and M. Irshad, *Bmc Biotechnol*, 2012, **12**, 1.

41. R. Li, X. Guo, K. Chen, J. Zhu, S. Li and J. Jiang, *J Microbiol Biotechnol*, 2009, **19**, 1439-1446.

42. D. C. Jones and R. A. Cooper, *Arch Microbiol*, 1990, **154**, 489-495.

43. M. Chen, P. Xu, G. Zeng, C. Yang, D. Huang and J. Zhang, *Biotechnol Adv*, 2015, **33**, 745-755.

44. G. Chandrasekaran, S. K. Choi, Y. C. Lee, G. J. Kim and H. J. Shin, *J Ind Eng Chem*, 2014, **20**, 3367-3374.

45. C. Zhang, W. Chen and P. J. Alvarez, *Environ Sci Technol*, 2014, **48**, 7918-7923.

46. A. L. Antaris, J. T. Robinson, O. K. Yaghi, G. Hong, S. Diao, R. Luong and H. Dai, *Acs Nano*, 2013, **7**, 3644-3652.

47. L. Wei, B. Wang, T. H. Goh, L.-J. Li, Y. Yang, M. B. Chan-Park and Y. Chen, *J Phys Chem B*, 2008, **112**, 2771-2774.

48. S. N. Kim, Z. Kuang, J. G. Grote, B. L. Farmer and R. R. Naik, *Nano Lett*, 2008, **8**, 4415-4420.

49. M. Y. Lobanov, N. Bogatyreva and O. Galzitskaya, *Mol Biol+*, 2008, **42**, 623-628.

50. B. Zhang, Y. Xing, Z. Li, H. Zhou, Q. Mu and B. Yan, *Nano Lett*, 2009, **9**, 2280-2284.

51. M. Lundqvist, I. Sethson and B.-H. Jonsson, *Langmuir*, 2004, **20**, 10639-10647.

52. P. Asuri, S. S. Bale, S. S. Karajanagi and R. S. Kane, *Curr Opin Biotech*, 2006, **17**, 562-568.

53. S. R. Saptarshi, A. Duschl and A. L. Lopata, *J Nanobiotechnol*, 2013, **11**, 1.

54. G. Zuo, X. Zhou, Q. Huang, H. Fang and R. Zhou, *J Phys Chem C*, 2011, **115**, 23323-23328.

Figure legends

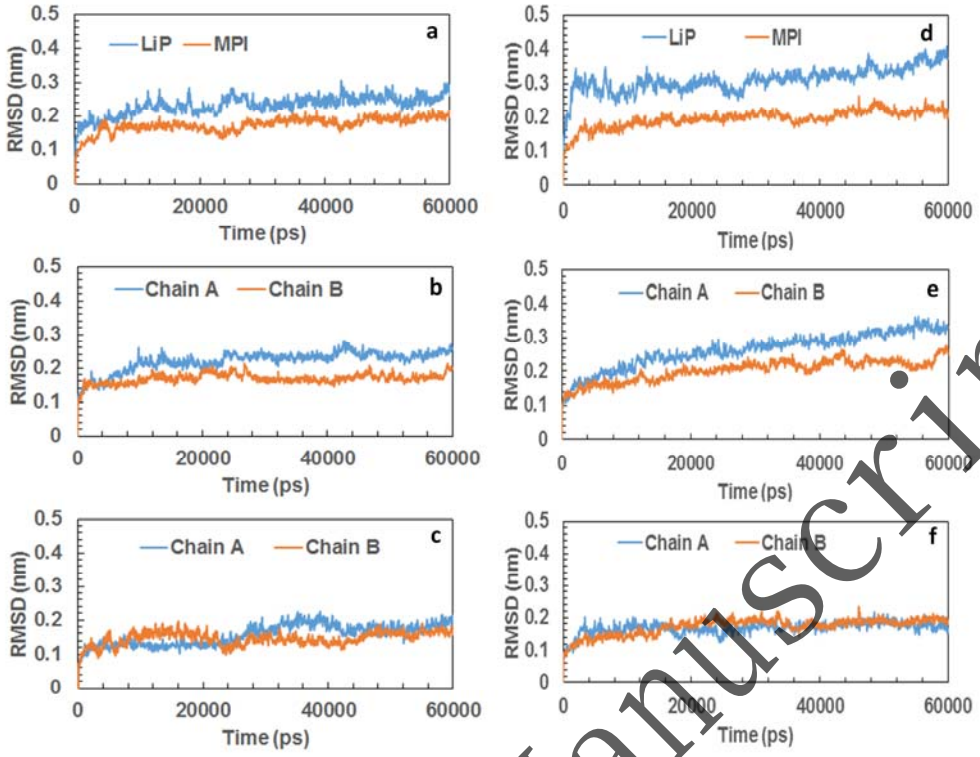

Figure 1. Backbone RMSD of LiP and MPI with time with and without the SWCNTs. a, the whole LiP and MPI without the SWCNTs; b, each chain of LiP without the SWCNTs; c, each chain of MPI without the SWCNTs; d, the whole LiP and MPI with the SWCNTs; e, each chain of LiP with the SWCNTs; f, each chain of MPI with the SWCNTs.

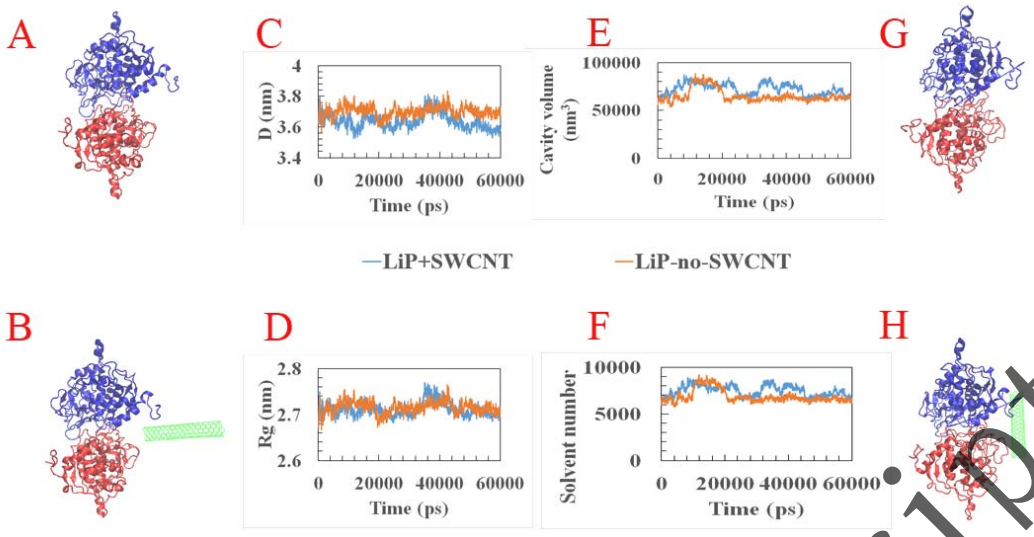

Figure 2. Conformational dynamics of LiP with and without the SWCNT with time. A, snapshot of LiP without SWCNT at 0 ns; B, snapshot of LiP with SWCNT at 0 ns; change in the distance between two chains (C), Rg (D), cavity volume (E) and solvent number overlapping the cavities (F) with time; G, snapshot of LiP without SWCNT at 60 ns; H, snapshot of LiP with SWCNT at 60 ns. Chains A and B are in blue and red, respectively.

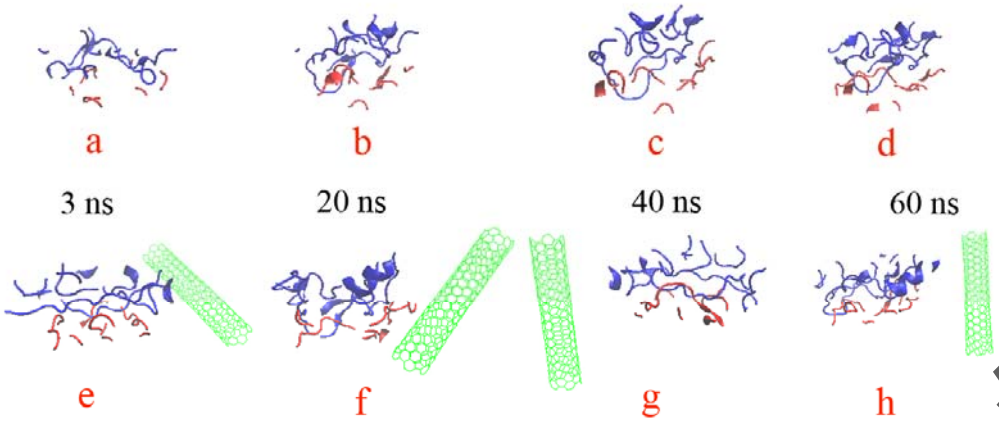

i

Time (ns)	LiP Without SWCNT		LiP With SWCNT	
	Atom number within 5 Å	Residues within 5 Å	Atom number within 5 Å	Residues within 5 Å
3	797	70	933	74
20	1094	82	1105	85
40	1042	80	1030	80
60	1163	82	1292	97

Figure 3. Evolution of 5 Å binding region within both chains A and B of LiP at 3, 20, 40 and 60 ns. Without SWCNT: a, b, c and d; with SWCNT: e, f, g and h; atom and residue number: i. Chains A and B are in blue and red, respectively.

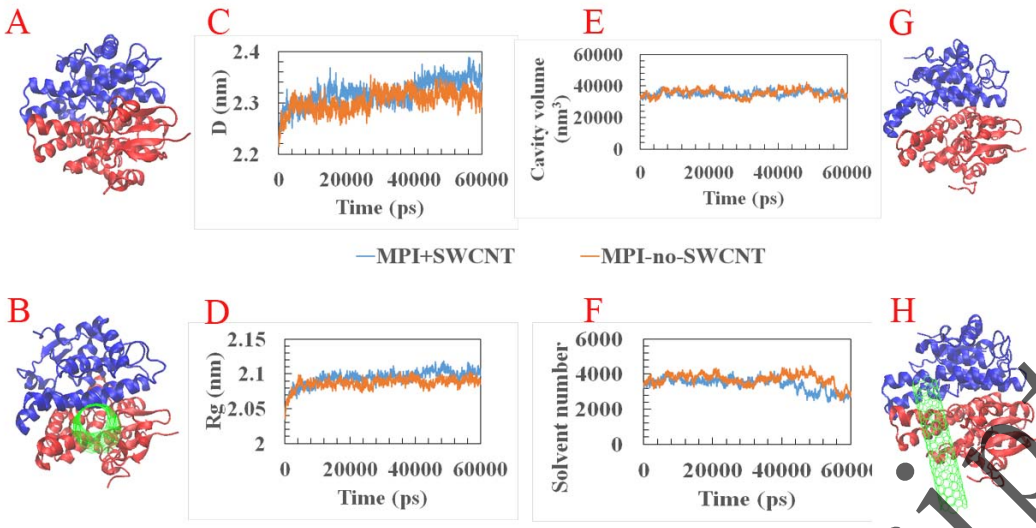

Figure 4. Conformational dynamics of MPI with and without SWCNT with time. A, snapshot of MPI without SWCNT at 0 ns; B, snapshot of MPI with SWCNT at 0 ns; change in the distance between two chains (C), Rg (D), cavity volume (E) and solvent number overlapping the cavities (F) with time; G, snapshot of MPI without SWCNT at 60 ns; H, snapshot of MPI with SWCNT at 60 ns. Chains A and B are in blue and red, respectively.

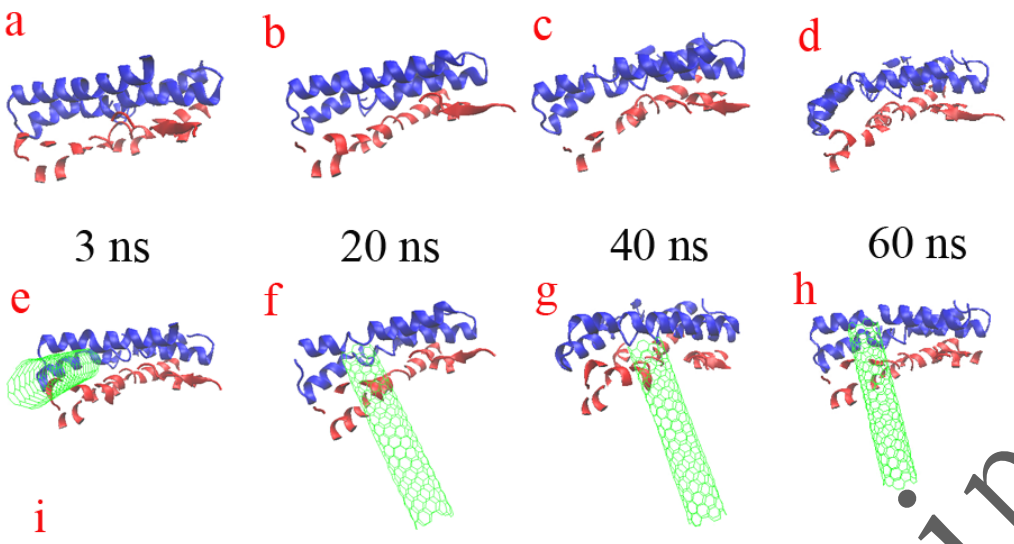

Time (ns)	MPI Without SWCNT		MPI With SWCNT	
	Atom number within 5 Å	Residues within 5 Å	Atom number within 5 Å	Residues within 5 Å
3	1861	105	1983	110
20	1892	111	1846	107
40	1808	106	1871	105
60	1915	107	1871	108

Figure 5. Evolution of 5 Å binding region within both chains A and B of MPI at 3, 20, 40 and 60 ns. Without SWCNT: a, b, c and d; with SWCNT: e, f, g and h; atom and residue number: i. Chains A and B are in blue and red, respectively.